Exploring the Effect of Aspect to Inform Future Earthcasts of Climate-Driven Changes in Weathering of Shale

P. L. Sullivan, Y. Godderis, Y. Shi, Yuqiao Gu, J. Schott, E. Hasenmueller, J. Kaye, C. Duffy, L. Jin, S. L. Brantley

AGU100 ADVANCING EARTH AND SPACE SCIENCE

JGR Earth Surface

RESEARCH ARTICLE
10.1029/2017JF004556

Key Points:
- Aspect-related differences in solar radiation in watersheds affect both the fluxes and extents of weathering from short to long timescales
- Reactive transport models of weathering suggest biolifting by vegetation slows mineral dissolution rates during weathering of shale
- Earthcasts of weathering fluxes must model not only geochemical processes but also erosion and biotic cycling rates

Supporting Information:
- Supporting Information S1

Correspondence to:
P. L. Sullivan,
plsullivan@ku.edu

Citation:
Sullivan, P. L., Goddéris, Y., Shi, Y., Gu, X., Schott, J., Hasenmueller, E. A., et al. (2019). Exploring the effect of aspect to inform future earthcasts of climate-driven changes in weathering of shale. *Journal of Geophysical Research: Earth Surface*, *124*, 974–993. https://doi.org/10.1029/2017JF004556

Received 18 JAN 2018
Accepted 8 MAR 2019
Accepted article online 18 MAR 2019
Published online 10 APR 2019

Exploring the Effect of Aspect to Inform Future Earthcasts of Climate-Driven Changes in Weathering of Shale

P. L. Sullivan[1], Y. Goddéris[2], Y. Shi[3], X. Gu[4], J. Schott[2], E. A. Hasenmueller[5], J. Kaye[3], C. Duffy[6], L. Jin[7], and S. L. Brantley[4]

[1]Department of Geography and Atmospheric Science, University of Kansas, Lawrence, KS, USA, [2]Géosciences Environnement Toulouse, CNRS – Observatoire Midi-Pyrénées, Toulouse, France, [3]Department of Ecosystem Science and Management, Pennsylvania State University, University Park, PA, USA, [4]Earth and Environmental Systems Institute and Department of Geosciences, Pennsylvania State University, University Park, PA, USA, [5]Department of Earth and Atmospheric Sciences, Saint Louis University, Saint Louis, MO, USA, [6]Department of Civil and Environmental Engineering, Pennsylvania State University, University Park, PA, USA, [7]Department of Geological Sciences, University of Texas at El Paso, El Paso, TX, USA

Abstract Projections of future conditions within the critical zone—earthcasts—can be used to understand the potential effects of changes in climate on processes affecting landscapes. We are developing an approach to earthcast how weathering will change in the future using scenarios of climate change. As a first step here, we use the earthcasting approach to model aspect-related effects on soil water chemistry and weathering on hillsides in a well-studied east-west trending watershed (Shale Hills, Pennsylvania, USA). We completed model simulations of solute chemistry in soil water with and without the effect of aspect for comparison to catchment observations. With aspect included, aqueous weathering fluxes were higher on the sunny side of the catchment. But the effect of aspect on temperature (0.8 °C warmer soil on sunny side) and recharge (100 mm/year larger on shaded side) alone did not explain the magnitude of the observed higher weathering fluxes on the sunny side. Modeled aspect-related differences in weathering fluxes only approach field observations when we incorporated the measured differences in clay content observed in augered soils on the two hillslopes. We also had to include a biolifting module to accurately describe cation concentrations in soil water versus depth. Biolifting lowered some mineral dissolution rates while accelerating kaolinite precipitation. These short-duration simulations also highlighted that the inherited differences in particle size on the two sides of the catchment might in themselves be explained by weathering under different microclimates caused by aspect—over longer durations than simulated with our models.

1. Introduction

One of the goals of critical zone scientists and observatories is to earthcast—that is, to project Earth's near-surface fluxes of water, solutes, gases, and sediments within the critical zone into the future (Duffy et al., 2014; Goddéris & Brantley, 2013; Murray et al., 2009; Pelletier et al., 2015). Depending upon the length of simulation, projecting these fluxes requires understanding the interaction of short timescale processes, such as plant-nutrient uptake and cycling, and long timescale processes such as soil development. In addition, each earthcast must be validated against observations; thus, models of earthcasting are often first used to reproduce measured water fluxes or soil chemistries observed today (e.g., Goddéris et al., 2013). Such model-data comparisons are useful not only as first steps toward projections into the future (which clearly are thought experiments that may or may not be successful projections) but perhaps more realistically as a way to understand the many coupled Earth system processes and how human actions might impact them.

Critical Zone Observatories, where soil pedons are well studied and instrumented (e.g., measurements of soil bulk chemistry, water chemistry, and moisture content) on hillslopes with different aspect, offer a platform to develop earthcasting models. Once calibrated, these models can be used to forecast the effect of climate change on water quantity and quality at that location. *Aspect* is used here to refer to the orientation of catchment hillsides with respect to Sun position (i.e., sunny vs shaded locations). We focus on hillslopes within a single catchment developed on a single parent material. In the targeted catchment, hillslopes are oriented with different aspects that cause differences in incoming energy and in soil hydrologic processes (e.g.,

timing, depth, and duration of water flow). Sun-facing slopes generally have higher radiative forcing and often lower moisture conditions (Chorover et al., 2011; Pelletier et al., 2013, 2018), which can further manifest as differences in the biogeochemical cycling of carbon and nitrogen (Hinckley et al., 2014; Kunkel et al., 2011). Given that solute fluxes in most natural environments are largely governed by water residence time and mineral-water interactions (e.g., Drever, 1988), changes in soil hydrologic processes related to differences in aspect are expected to alter weathering fluxes. Hillslopes are fundamental integrators of water, energy, and biogeochemical fluxes (Fan et al., 2018). Thus, illuminating aspect-driven differences in the behavior of hillslope processes will provide the platform to earthcast at watershed and continental scales by defining the key processes that must be included (Sullivan et al., 2018).

To forecast potential hillslope weathering processes, we develop an earthcasting model to simulate the impact of differences in radiative forcing on weathering and geochemical fluxes at the well-studied, east-west trending Susquehanna Shale Hills Critical Zone Observatory (SSHCZO), Pennsylvania, USA (Figure 1). Toward this end, we develop an aspect module for the existing hydrologic code Flux-Penn State Integrated Hydrologic Model (PIHM, Shi et al., 2013) to simulate the microclimate-driven differences on two sides of the catchment. To simulate the effects on soil water solute concentrations, solute fluxes, and weathering rates, we linked microclimate outputs from Flux-PIHM (e.g., evapotranspiration, soil temperature, soil moisture, and soil water fluxes) to the geochemical code WITCH (Goddéris et al., 2006, 2010; 2013) (Figure 2). We parameterized the model with observations from SSHCZO that show that soils are more chemically depleted and have less clay content on the shaded hillslope as compared to the sunny one (Ma et al., 2010, 2013), and we used soil water chemistry collected from 2006 to 2012 at the same locations as measurements of bulk soil chemistry. The model was used to simulate soil water solute concentrations, fluxes, and elemental release rates of weathered elements to solution in soil pedons and then compared to observations (e.g., soil water solute concentrations on the two hillslopes, Herndon, 2012). One important observation we sought to understand is the measurement of higher elemental release rates on the sunny side of the catchment (Ma et al., 2013). In addition, to simulate variations in pore water chemistry versus depth, we included a module describing *biolifting*—the uptake of inorganic nutrients at depth by plants and the return of these nutrients to surface soils (Jobbágy & Jackson, 2001; Lucas, 2001). The biolifting module incorporated vegetation cycling to fit the soil water solute observations. We then ran sensitivity analyses to inform how such earthcast models respond to the interaction between climate change, vegetation cycling, and particle size distribution. Once the model successfully simulated today's weathering fluxes and rates, we used it to elucidate past processes controlling weathering extent.

2. Background

Our site is a 7.9-ha V-shaped temperate forested catchment (30-year average precipitation and temperature at 107 cm/year and 10 °C, respectively; USC00368449 location, NOAA 2007) that overlies the Rose Hill Shale formation (Clinton group) within the Valley-and-Ridge Physiographic Province of the Appalachians. The catchment is oriented east-west and is bisected by an ephemeral stream. Given the location in the Northern Hemisphere, we simplify our descriptions by referring to the hillslope that faces south as the *sunny* hillslope and the hillslope that faces north as the *shaded* hillslope. Soils on both hillslopes are developed from the same Rose Hill shale parent material. The bulk mineralogy of this shale rock is composed of Mg-rich silicate minerals illite and “chlorite” (where quotation marks are used to indicate the presence of not only chlorite but also vermiculite and hydroxyl-interlayered vermiculite) as well as quartz, with minor contributions of feldspar (K-spar and plagioclase; Jin et al., 2010; Table SM1 in the supporting information) and variable amounts of carbonate that are generally low throughout most of the watershed (Jin et al., 2010).

The soils at the SSHCZO were formed from shale colluvium or residuum (Lin et al., 2006). Soil thickness varies both along and between hillslopes, with soils thickening from the ridge top toward the valley floor and in swales compared to the planar slopes (Lin, 2006; Figure 1). We focused this study on midslope positions along the generally planar slopes on both the sunny and shaded hillslopes because they consist of the same soil series (loamy-skeletal Weikert series) and are derived from the same parent material. Interestingly, soil residence times are 2–3 times greater and soils are more weathered on the shaded side of the catchment (determined using U-series isotopes; residence times of sunny side midslope soils = 12 ± 3 ka, shaded side 33 ± 24 ka; Ma et al., 2010, 2013). To account for this difference in weathering, we analyzed soils

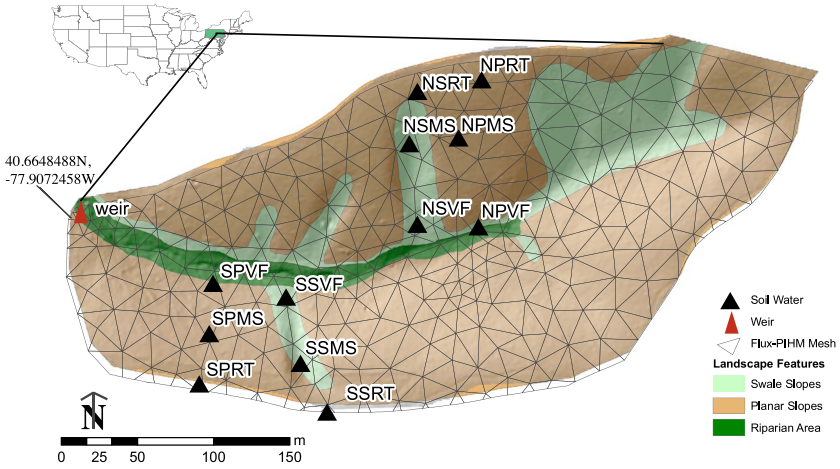

Figure 1. The model in this paper focused on the Susquehanna Shale Hills Critical Zone Observatory (SSHCZO), Pennsylvania (USA). Measurement sites (solid triangles) included observations of soil water and bulk geochemistry for northern (N) and southern (S) portions of the basin. Acronyms for sampling locations refer to samples collected on planar hillslopes (P) and swales (S) at ridgetop (RT), midslope (MS), and valley floor (VF) locations. Measurements were coupled with the Flux-PIHM hydrologic model (gray mesh) and the WITCH geochemical code to relate climatic controls to soil water solute concentrations. PIHM = Penn State Integrated Hydrologic Model.

for particle size distribution by wet sieving (see supporting information for specific details on analysis; Table 1). Our approach did not use a dispersion agent; rather, it used centrifugation instead of settling. We acknowledge that this approach may cause uncertainty in the relative amounts of silt and clay given that coarse clay may settle with centrifugation and aggregated clay may act like silt. We do not quantify this uncertainty, but further investigation of the issue is warranted given the role of clay in our analysis. Also, when calculating the percent particle size distribution, we include rock fragments to best represent the soils at SSHCZO because all of our analyses are aimed at understanding mass balance and to do this requires incorporation of all particle sizes that emerge from underlying rock into the soil. Four particle

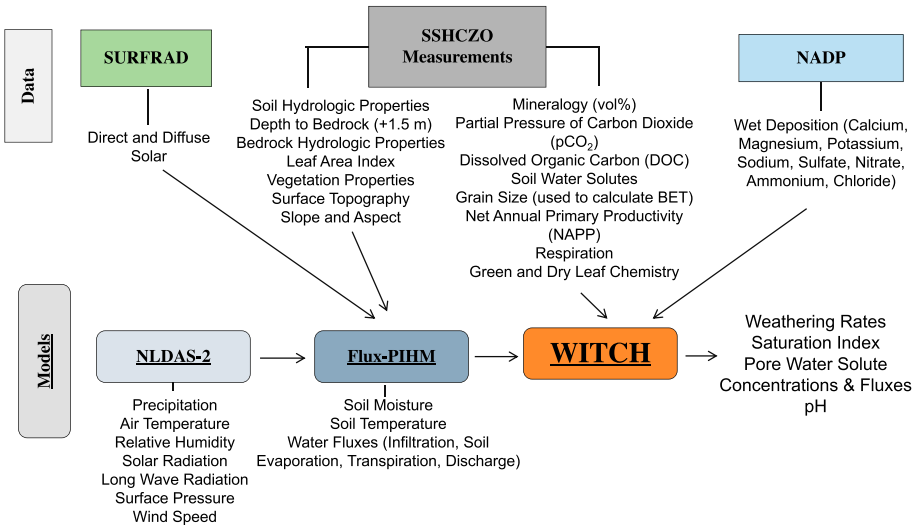

Figure 2. Work flow for linking data and models in our analysis. Meteoric forcing for Flux-PIHM was derived from the NLDAS-2 and the surface radiation network (SURFRAD), while static inputs (e.g., hydrologic properties and land cover) were prescribed from field measurements. Hydrologic forcing from Flux-PIHM, geochemical data from the SSHCZO, and precipitation chemistry (National Atmospheric Deposition Program; NADP) served as the inputs to WITCH. PIHM = Penn State Integrated Hydrologic Model; NLDAS-2 = Phase-2 North American Land Data Assimilation System.

Table 1
Particle Size Distribution at the Midslope Positions of Shale Hills

Depth (cm)	Rock fragment (%)	Sand (%)	Silt (%)	Clay (%)
Sunny				
4.0	15%	28%	40%	17%
11.5	30%	22%	40%	7%
18.5	27%	24%	39%	10%
28.5	23%	27%	38%	11%
33.0	44%	14%	34%	8%
37.5	49%	18%	23%	10%
Shaded				
5.0	41%	34%	22%	3%
15.0	54%	21%	22%	3%
25.0	57%	18%	22%	3%
35.0	64%	14%	19%	4%
45.0	59%	19%	19%	3%
55.0	80%	9%	9%	2%

Note. Particle size distribution method is detailed in Supplemental Material section 1.2.

size classes (clay, silt, sand, and rock) are often used to estimate surface area for the determination of weathering rates (e.g., Goddéris et al., 2006; Sverdrup, 1996; explained in section 3.2 below). Published relationships allow estimation of the Brunauer-Emmett-Teller surface area and relate it to the total surface area (determined from clay, silt, sand, and rock fragments). When total surface area is coupled with soil moisture, weathering rates can be determined. When the rock fragments were included, the depth-weighted average clay content on the sunny slope was 10.7%, while on the shaded slope it was 3.8%; if only fine Earth material was included in the particle size distribution calculations, then the clay content on both hillslopes was observed to be larger, with values on the sunny slope still exceeding those on the shaded slope (15.1% and 9.8%, respectively). Although the difference in clay content between the hillslopes is sensitive to the presence of rock fragments (which are typically excluded in studies that focus on fine Earth material), we retain the rock fragments on purpose in order to account for the relationship between total surface area and Brunauer-Emmett-Teller surface area for weathering rates.

One reason we focus on soils on the planar slopes was to reduce hydrologic complexity: for example, we are not modeling the convergent flow that occurs in swales. To first approximation, unsaturated soils on planar slopes are characterized by vertical downward flow. Horizontal flow occurs at the base of pedons—the interface of soil with underlying rock—and sometimes at the interface of the A and B horizons when saturation occurs (Brantley et al., 2013; Jin et al., 2011; Lin, 2006; Sullivan, Hynek, et al., 2016; Sullivan, Ma, et al., 2016; Thomas et al., 2013). In this modeling effort, we focused on the changes in water chemistry versus depth that were dictated by unsaturated flow conditions. The model thus posits strictly vertical, downward flow through the pedons.

We simulated land-atmosphere, hydrologic, and geochemical fluxes rather than direct observations of water flow because such simulations provide long-term *data* without the patchiness of experimental observations (Figure 1). We used simulated land-atmosphere and hydrologic data to parametrize WITCH and (1) to run the model over the duration for which we had soil water chemistry data (2006–2012); and (2) to determine soil moisture, fluxes, and temperature values in the vicinity of the soil water lysimeters and soil bulk chemistry observations. Flux-PIHM was previously calibrated and validated with observations from SSHCZO to simulate soil moisture, groundwater table position and stream discharge (Shi et al., 2013); we use this same model but include a module for aspect (see supporting information section 2).

3. Methods

3.1. WITCH-Baseline Model

A cascade modeling approach was used to develop a baseline model (Figure 2). We use the term "cascade" to refer to the unidirectional linkage between the meteorological forcing from the Phase-2 North American Land Data Assimilation System (NLDAS-2; http://www.hydroterre.psu.edu/), the fully coupled land surface Penn State Integrated Hydrologic Model (Flux-PIHM; Shi et al., 2013), and the geochemical box model WITCH (Goddéris et al., 2006, 2010; 2013). Flux-PIHM was calibrated and validated with data from SSHCZO (see Shi et al., 2013). We used the same static inputs for our simulations and included spatially explicit field-measured soil and bedrock hydrologic properties (e.g., porosity and ability to retain water under gravity), depth to bedrock (Lin et al., 2006), forest cover (Meinzer et al., 2013), vegetation properties (Shi et al., 2013), and topography (Shi et al., 2013). Soil hydraulic properties were assigned in Flux-PIHM based on a spatial survey of soil series at SSHCZO (Lin, 2006). Based on that study, soils on midslope planar locations on both sides were identified as the Weikert soil series and were prescribed with the same hydraulic properties derived from average field measurements. The Flux-PIHM output to WITCH included soil moisture, soil water fluxes, and soil temperature across three soil layers (bottom of each layer = 5, 25, and 70 cm, that is, the average depth to the bottom of each horizon) within each of the given 561 grid cells in Flux-PIHM (Figure 1). The average hydrologic and temperature forcings from grids cells that represent the sunny and shaded midplanar slope positions were used for the simulations. We parameterized the

model with NLDAS-2 precipitation data for 2006–2012 (averaged 1087 ± 160 mm). At SSHCZO, because roughly 25% of the precipitation is snow delivered between December and March (Thomas et al., 2013), Flux-PIHM uses a simple temperature index to represent snow melt physics (Kumar, 2009). Such simple representations of snowmelt-runoff dynamics can lead to deviations in the timing and quantity of projected compared to observed discharge (Shi et al., 2013). We also used existing physical and biogeochemical data (Table 1; Tables SM1—SM4) and then validated the model using soil water chemistry from lysimeters at the midslope positions of the sunny and shaded hillslopes (Table SM5). Soil water can generally not be sampled with suction lysimeters at the site between late July and early September given the high evapotranspiration demand compared to precipitation. For this reason, we focus the model validation on the time periods when solutes were measured on soil waters (March–November, excluding late July through early September) instead of seasonal or annual averages.

3.2. Model Soil Composition

For the WITCH-Baseline model, as in SAFE and PROFILE geochemical models (Sverdrup, 1996), the total surface area (m^2/m^3) is estimated using a geometric-parametric law where the bulk density of the soil (g/m^3) is multiplied by the fractions of clay, sand, silt, and rock fractions weighted with empirical values assigned to the respective proportions: 8.0: 2.2: 0.3: 0.05 (Sverdrup & Warfvinge, 1995). Thus, the total surface area is prescribed based on the particle size distribution with an empirical approach. In our simulations, the value is then distributed equally among the minerals based on volume abundance of each mineral in each layer such that no mineral is favored based on size class. For this reason, the reactive surface area of each mineral is a linear function of their volumetric abundance. For example, the total reactive surface area for the deepest soil on the sunny hillslope was set in the model to equal 1.79×10^6 m^2/m^3 because we assumed a bulk density of 1.3 g/cm^{-3} (measured using 5.4-cm-diameter brass core in triplicates, Lin, 2006). Bulk density, determined from soil cores, included the shale rock fragments. Rock fragments were included in the large particle size fraction on purpose because we compare the calculated soil chemistry directly to the protolith chemistry. To do this requires that all size fractions of material be included.

3.3. Model Mineral Dissolution and Precipitation

Soil mineralogy was determined on bulk soil samples using qualitative X-ray diffraction with standard clay separation used to identify specific clay minerals (Jin et al., 2010). Mineralogy was combined with bulk geochemistry to estimate mineral abundances versus depth for use in WITCH. Here Mg-rich clays, illite, and chlorite represent the largest pools of reactive minerals at SSHCZO, followed by kaolinite and feldspar (Table SM1). Values of solubility products and dissolution rate constants for minerals were selected after a critical review of available experimental data (see Tables SM2 and SM3; Goddéris et al., 2006, 2010). The dissolution or precipitation rate (F_g; mol/s) of mineral g was described by a rate equation derived from Transition State Theory (Schott et al., 2009):

$$F_g = A'_g * \left[\sum_l k_{l,g} * \exp\left(\frac{-E^l_{a,g}}{R*T} \right) * a_l^{n_{l,g}} * f_{\text{inh}} \right] * \left(1 - \Omega_g^{1/s} \right). \quad (1)$$

The rate is a function of the reactive surface area (A', m^2); the sum of parallel dissolution reactions promoted by four species (l): H^+, OH^-, H_2O, and organic acids; and a function of the degree of departure from equilibrium for mineral g ($1\text{-}\Omega_g^{1/s}$). Ω_g is the saturation index. Here a and n are the activity and reaction order, respectively, of the lth species, k (mol m^{-2}/s) is the dissolution rate constant, E_a is the activation energy, R is the universal gas constant, T is the temperature, and f_{inh} accounts for inhibitory effects. The degree of departure from mineral equilibrium is solved by evaluating the solution saturation state Ω_g with respect to mineral g and by using a value of Temkin's coefficient (s). All thermodynamic calculations in the study, including a_i and Ω_g, were performed using the Lawrence Livermore National Laboratory database (llnl.dat) for aqueous species and thermodynamic parameter values for the solid phases listed in the Table SM3. For SSHCZO simulations, WITCH used solute concentrations, relying on the assumption that soil solutions are generally dilute enough that activity corrections are minimal in temperate environments.

The pH values of the soil waters are calculated by solving the charge balance at each depth and time step, accounting for the production or consumption of alkalinity through mineral dissolution or precipitation, the belowground partial pressure of CO_2, and the release of protons by organic acids (Goddéris et al., 2010).

Specifically, light organic acids within each soil layer were prescribed (Goddéris et al., 2010) based on the average dissolved organic carbon (DOC) concentrations measured in the soil water with depth at each site (Andrews et al., 2011). Light organic acids are assumed in the model to dissociate ($RCOOH \rightarrow RCOO^- + H^+$) according to a dissociation constant developed by Sverdrup and Warfvinge (1995).

The belowground partial pressure of CO_2 (pCO_2) is prescribed at each time step in the model as a function of depth and location. The values of pCO_2 were based on 2 years of approximately biweekly field measurements for the south planar midslope pedon, that is, on the shaded hillslope (2008–2011; Hasenmueller et al., 2015). Measurements were available at approximately 10 cm depth intervals down to auger refusal. Such data were also available for the sunny hillslope for a different year (i.e., 2013; Hasenmueller et al., 2015). A comparison of the soil gas data for the sunny versus the shaded hillslopes (albeit for different years) revealed little effect of aspect: in general, the pCO_2 values increased with soil depth and tracked the growing season, with values increasing during the spring and early summer and then decreasing in the fall. Functions were fit to the pCO_2 data for the shaded hillslope on a subdaily time step, and concentrations were interpolated between depths (Figure 3).

By accounting for pCO_2 and DOC we take into consideration the impact of root and microbial respiration as well as the impact of organic acid production on chemical weathering. Thus, the simulated soil water pH values vary as a function of: 1) the precipitation or dissolution of minerals, 2) inputs of slightly acidic meteoric water, and 3) generation of protons from the inclusion of organic acids and soil pCO_2 data in the model. The pH values of meteoric water inputs were set equal to 4.8 ± 0.4 as calculated by the model from charge balance from measured precipitation chemistry for 2006–2012 (National Atmospheric Deposition Program, 2013).

3.4. Weathering Fluxes

Mg weathering fluxes (mmol Mg/year) were calculated from the model as the average daily solute mass outflux (f) from the bottom of the soil profile integrated over a year:

$$f_{Mg} = \sum_{i=0}^{365} V \times C_{Mg} \tag{2}$$

Here V is the daily volumetric water outflux (m^3/d) and C_{Mg} is the average molar concentration of Mg in soil water (mmol Mg/m^3) each day, both of which were modeled at the bottom of the profile.

3.5. New WITCH Modules

3.5.1. WITCH + Aspect Model

To simulate the effect of aspect, a topographic solar radiation module was added to Flux-PIHM (see supporting information section 2). Values for direct and diffuse solar radiation obtained from the NOAA surface radiation network (SURFRAD; http://www.esrl.noaa.gov/gmd/grad/surfrad/) were used in simulating aspect.

3.5.2. WITCH + Aspect + Vegetation Model

Plants are known to significantly influence the accumulation of certain elements (e.g., K and Ca; Herndon, Dere, et al., 2015, Herndon, Jin, et al., 2015; Jobbágy & Jackson, 2001; Lucas, 2001) in near surface soils through biolifting—the vertical uplift and recycling of cations by vegetation—and the short-term processes of accumulation, storage, and release. The original source of these elements is either derived from mineral weathering or atmospheric deposition. Given that WITCH already accounts for wet deposition chemistry (Figure 2), the only way for WITCH to reproduce the observed depth profiles was to include a process such as biolifting that changes the depth distribution of solutes. We therefore developed a biolifting module, here referred to as a vegetation cycling module, in WITCH accounted for the impact of biolifting on soil water chemistry and mineral saturation indices. We focused this module solely on the elements associated with litter production/decay. Specifically, to model elemental release rates (r; mol m^{-2}/s) from litter we used a so-called Q_{10} law:

$$r = r_{mg} * E_e * Q_{10}^{(T-T_{25})/10} \tag{3}$$

Here r is calculated as a function of the release rate of Mg (r_{mg}; mol m^{-2}/s), the elemental ratio (E_e) in leaf litter for a given element (e; Ca, Si, and K) with respect to Mg, the activation energy or temperature coefficient (Q_{10}) describing the variation in litter decomposition as a function of temperature (T; °C), and the

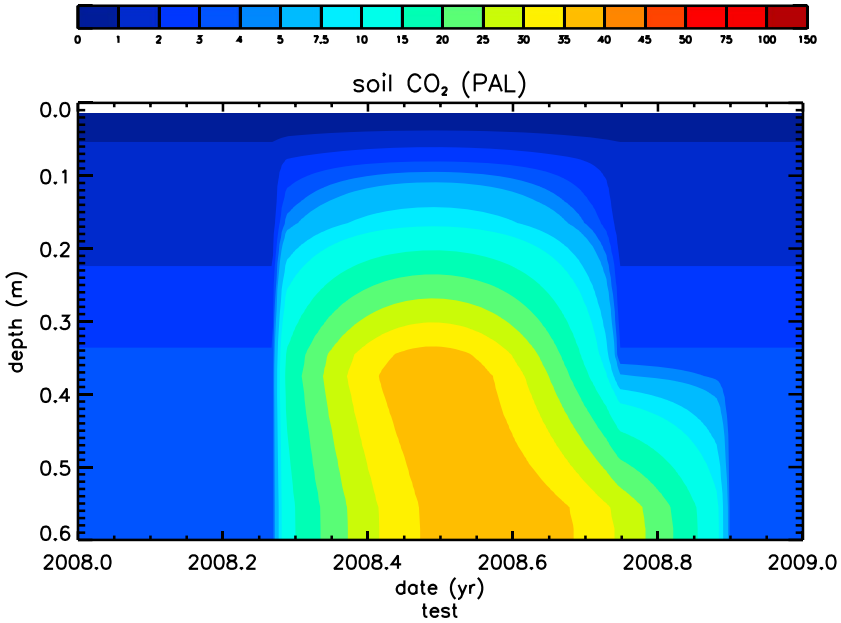

Figure 3. Modeled values of concentrations of CO_2 in the soil atmosphere as a function of depth (0–60 cm) and time for the midslope soil on the shaded hillslope. The date indicates decimal year (i.e., 0.2 represents 2.4 months), and the soil CO_2 is color coded as present atmospheric level (PAL). The modeled values are based on measurements as described in text.

reference temperature (T_{25}; °C). The value of r_{mg} was estimated for soil at a depth of 5 cm as the ratio of the annual net carbon (C) produced in leaf litter (220 g C·m^2·year^{-1}; Smith, 2013) from 2010 at the SSHCZO and the average Mg concentration per unit C in the leaf litter (0.004 g/g; Herndon, Dere, et al., 2015). The elemental ratio prescribed for K: Ca: Si: Mg in leaf tissues was 1.16: 4.43: 2.40: 1.00 (Herndon, Dere, et al., 2015).

To examine how aspect and vegetation may work in concert, we tested nutrient cycling on our model runs with aspect. We used a Q_{10} value of 1.5, which fell within the range (2.2 ± 0.9) of Q_{10} values observed in temperate regions (Chen & Tain, 2005). The value of 1.5 was tuned in the model to achieve soil water solute concentrations that most closely reproduced Ca, K, and Si. It is important to note that we developed this module to better simulate K, Ca, and Si soil water solute concentrations; it is possible that other processes such as those related to organic acid generation during soil organic matter decay or root exudation might have been included in the model and might have provided adequate simulations of the depth profiles of the target elements. For example, solute concentrations might be influenced by these alternate phenomena that were not entirely treated by the model: (1) organic-mineral chelation, (2) ligand-promoted dissolution, and (3) Al inhibition (e.g., Lawrence et al., 2014). WITCH does account for the effect of organic acid-driven chemical weathering (section 3.3), but our parameterization of light molecular weight organic acids as DOC at a given depth was held constant over time, and WITCH does not explicitly account for organic-metal complexation.

Plants take up nutrients in soil solutions at all depths at and above the maximum rooting depth, while those nutrients are ultimately released in the top soil layers by litter decomposition. This process generates a vertical profile in which the nutrients in the top layer are maintained at higher concentrations than at depth (the effect referred to here as biolifting). In this first attempt at accounting for this effect, we assume that the integrated uptake along the root zone equals the released flux at the top at each time step. We assume that uptake and nutrient release by decomposition is coupled because solar radiation governs photosynthesis, growth, transpiration, and temperature. We also assume that temperature drives decomposition and kinetics. Thus, we use seasonal variation in soil temperature at 5 cm as a proxy for regulating uptake and decomposition. In systems that have distinct seasonal changes in temperature and fairly constant inputs of meteoric water such as SSHCZO (Figure 4), this simplification is used to represent the general impact

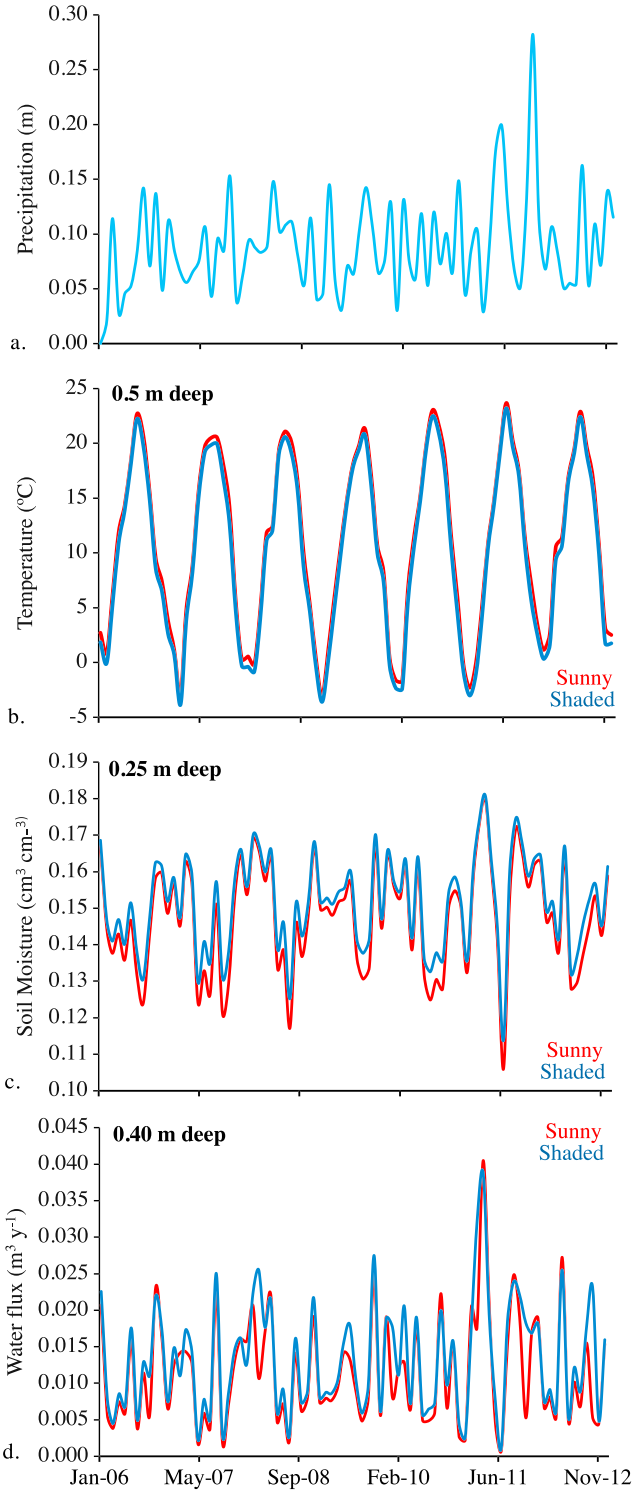

Figure 4. Average monthly hydrometeorological forcing for WITCH Baseline + Aspect on the sunny (red) and shaded (blue) hillslopes: (a) precipitation, (b) soil temperature at 0.05-m deep, (c) soil moisture at 0.25-m deep, and (d) vertical waterfluxes at 0.4-m deep.

of nutrient cycling. Future model development could account for variations in the balances of the fluxes on a seasonal basis.

Elemental uptake by vegetation was constrained to occur in two portions of the soil profile: (i) ~90% of elemental uptake occurred evenly between 0- and 18.0-cm deep in the soils and (ii) ~10% of elemental uptake occurred evenly between 18.1- and 60-cm deep in the soil. All elemental release from decomposing litter occurred within the top 6 cm of the profile. In other words, elemental uptake occurred across the entire profile, while elements were released from decomposition only to the top of the soil profile. This modeling scheme is in accordance with the observed root density and water uptake at SSHCZO: the majority of roots are observed within the top 20 cm of the soil profile, though roots have been observed to at least 180 cm (Hasenmueller et al., 2017). In addition, most trees utilize water from the upper 40 cm (Gaines et al., 2015).

3.6. Model-Data Comparison

The model was validated using two techniques: (1) a graphical comparison of simulated and observed (2006–2012) soil water solute concentrations at 10-cm depth increments over the 60 cm soil profile on both sides of the catchment, and (2) calculation of the normalized Nash-Sutcliffe efficiency (NNSE) index (Nossent & Bauwens, 2012). The NNSE index varies between 0 and 1, where 1 indicates a perfect ability for the model to reproduce the mean (Gupta et al., 2009). Here we calculate the integrated NNSE for all depths over time on each hillslope (e.g., sunny and shaded) to provide one value of performance per solute per pedon for each simulation.

4. Modeling Results

4.1. WITCH-Baseline Model

4.1.1. Hydrology

In the baseline WITCH model, uniform radiative forcing was used across the catchment. Without including aspect explicitly, the soil temperature at a depth of 5 cm estimated by Flux-PIHM differed by 0.1 °C on the hillslopes (sunny side = 10.8 °C; shaded side = 10.7 °C; Table 2). Both soil water recharge and soil moisture were slightly higher on the shaded side of the catchment (Table 2). The differences in temperature and recharge, 0.1 °C and 0.01 m/year, were so small that they can best be considered as the error in the average calculations across all the soil pixels.

4.1.2. Weathering Fluxes

The WITCH-Baseline model simulated the observed pH value for the sunny hillslope below 30-cm depth and the progressive rise in pH with depth (Figure 5a). On the other hand, the baseline simulation for the shaded hillslope does not match the soil water pH profile. Specifically, the simulated pH stays below 4 across the entire profile while the observed values are roughly constant at 4.5. It is interesting to note that with the exception of values measured at 30-cm deep on the shaded slope, the increase in pH with depth is greater in both observations and simulations on the sunny hillslope compared to the shaded one. These patterns are the consequence of a lower supply of cations by weathering on the shaded hillslope relative to the sunny one because of the prescribed differences in clay content of the two sides. The elevated pH observed at 30-cm depth on the shady slope might arise from preferential flow paths

Table 2
Flux-PIHM Recharge[a] and Temperature Predictions and WITCH Model Outputs (Mg Soil Water Concentrations at 40 cm, Mg Flux, and Total Extent of Weathering)

	NPMS	SPMS
[b]WITCH-Baseline model	Sunny	Shaded
Average temperature (°C)	10.8 ± 0.5	10.7 ± 0.4
Average annual min temperature (°C)	−10.7 ± 2.4	−10.2 ± 2.4
Average annual max temperature (°C)	27.9 ± 2.1	27.8 ± 2.2
Average annual recharge (m/year)	0.68 ± 0.04	0.69 ± 0.13
Mg flux (mmol Mg/year)	33.7 ± 0.1	17.1 ± 0.2
Mg soil water concentration (mmol/L)	58.9 ± 22.8	27.6 ± 12.4
Extent of weathering (%)	41 ± 3	63 ± 3
[c]WITCH + Aspect		
Average temperature (°C)	10.8 ± 0.5	10.0 ± 0.4
Average annual min temperature (°C)	−10.6 ± 2.3	−10.6 ± 2.5
Average annual max temperature (°C)	27.5 ± 2.0	26.8 ± 2.1
Average annual recharge (m/year)	0.63 ± 0.02	0.73 ± 0.14
Mg Flux (mmol Mg/year)	35.3 ± 0.3	16.8 ± 0.2
Mg soil water concentration (mmol/L)	62.5 ± 22.8	25.6 ± 12.49
Extent of weathering (%)	37 ± 4	62 ± 2
[d]WITCH + Aspect + Vegetation		
Mg flux (mmol Mg/year)	31.9 ± 0.2	15.2 ± 0.1
Mg soil water concentration (mmol/L)	57.0 ± 17.4	23.0 ± 10.6
Extent of weathering (%)	32 ± 1	51 ± 3
[e]WITCH + Aspect + Vegetation + Clay		
Flux (mmol Mg/year)	17.1 ± 0.2	30.6 ± 0.2
Mg soil water concentration (mmol/L)	28.8 ± 13.8	47.8 ± 19.0
Extent of weathering (%)	15 ± 3	90 ± 9

Note. NPMS = North Planer Midslope; SPMS = SouthPlaner Midslope.
[a]Recharge is defined as the water vertically infiltrating to a depth > 70 cm. [b]WITCH-Baseline condition (without aspect), [c]WITCH + Aspect (altered temperature and hydrologyregimes from Flux-PIHM on the shaded side), [d]WITCH + Aspect + Vegetation (included cycling onnutrients by vegetation), [e]WITCH + Aspect + Vegetation + clay content (3% on sunny side and 10% on shaded side).

between soil horizons A and B, as identified by Jin et al. (2011) using water isotopes and Mg and Cl concentrations. When such flows include a horizontal component, they can only be simulated in Flux-PIHM once the entire pedon is saturated and can maintain horizontal flow; thus, the model underrepresented the impact of horizontal flow paths in the soil on the soil water chemistry depth profiles.

Like the pH in deeper soil layers, the modeled dissolved Mg concentrations fall within the range of measured soil solution data for the sunny hillslope but not the shaded one (Figure 6a) at depths greater than 20 cm. On the sunny hillslope, Mg concentrations increased with depth to a greater degree in the simulated concentrations compared to the observed values. On the shaded hillslope, the observed concentrations have a much greater degree of variability compared to the sunny side and the simulation consistently underestimated the Mg concentrations except at a depth of 30 cm. This difference in observed versus simulated soil water concentrations on the two hillslopes could arise from differences in preferential flow paths related to aspect. Where moisture regimes differ with aspect it can alter the dynamics of preferential flow paths (e.g., Casanova et al., 2000; Geroy et al., 2011; Hinckley et al., 2014). For example, shaded slopes can have a greater degree of preferential flow development than sunny hillslopes (see references in Pelletier et al., 2018 review). For soil profiles at all depths on both hillslopes, the model also approximated the observed values Si and Al to a depth of 30 cm and then overestimated Al at greater depths (Figures 6c and 6d). Likewise, the model consistently underestimated Ca and K by 2 orders of magnitude (Figures 6b and 6e and Figure 7).

Concentrations of all simulated solutes showed similar seasonal patterns: elevated values in the drier months between April and September and lower values in the wetter months between November and March, here concentrations generally increased with depth (Figure 7). The elevated solute concentrations during the warmest months resulted in part from a concentrating effect as soil moisture decreased during the growing season when evapotranspiration was highest. Conversely, during the winter and spring, inputs of meteoric water and reduced evapotranspiration increased soil moisture and diluted soil water solute concentrations (Figure 4c).

Simulating Mg and Si dynamics is the first order priority in modeling chemical weathering at SSHCZO because the mineralogy is dominated by Mg-rich silicate minerals (Li et al., 2017). Thus, if we can simulate Mg and Si it provides a degree of confidence that the model represents the factors that control chemical weathering of dominant minerals in the catchment. Overall, the higher NNSE values of Mg and Si compared to other soil water solutes (Table 3) in the WITCH-Baseline indicate the model best predicted Mg and Si. In addition, NNSE values indicated that the model does a slightly better job reproducing Mg and Si for the sunny slope compared to the shaded one. When we compared weathering fluxes from these hillslopes, the WITCH-Baseline simulation revealed that the net flux of Mg on the sunny hillslope was nearly twice that of the shaded one (33.7 and 17.1 mmol Mg/year, respectively; Table 2), and this was largely due to the inherent difference in the clay content of the two hillslopes.

4.1.3. Mineral Weathering

The WITCH-Baseline model calculated that illite, chlorite, albite, and K-feldspar should be dissolving but that kaolinite is near equilibrium or supersaturated with respect to kaolinite in the soils (Figures 5b–5d). As calculated by the WITCH-Baseline model, the dominant source of Mg and Si to soil water was chlorite because it dissolved about an order of magnitude faster than illite on both hillslopes (Figures 5c and 5d). Dissolution rates of all minerals were calculated to be highest between April and September when both CO_2 concentrations and soil temperatures were elevated (Figure 3). The modeled rates of dissolution are small: for example, it would take approximately ~5.6 ka for 2.7 vol % chlorite to completely dissolve from the soil profile if we just use a simple batch dissolution mode calculation.

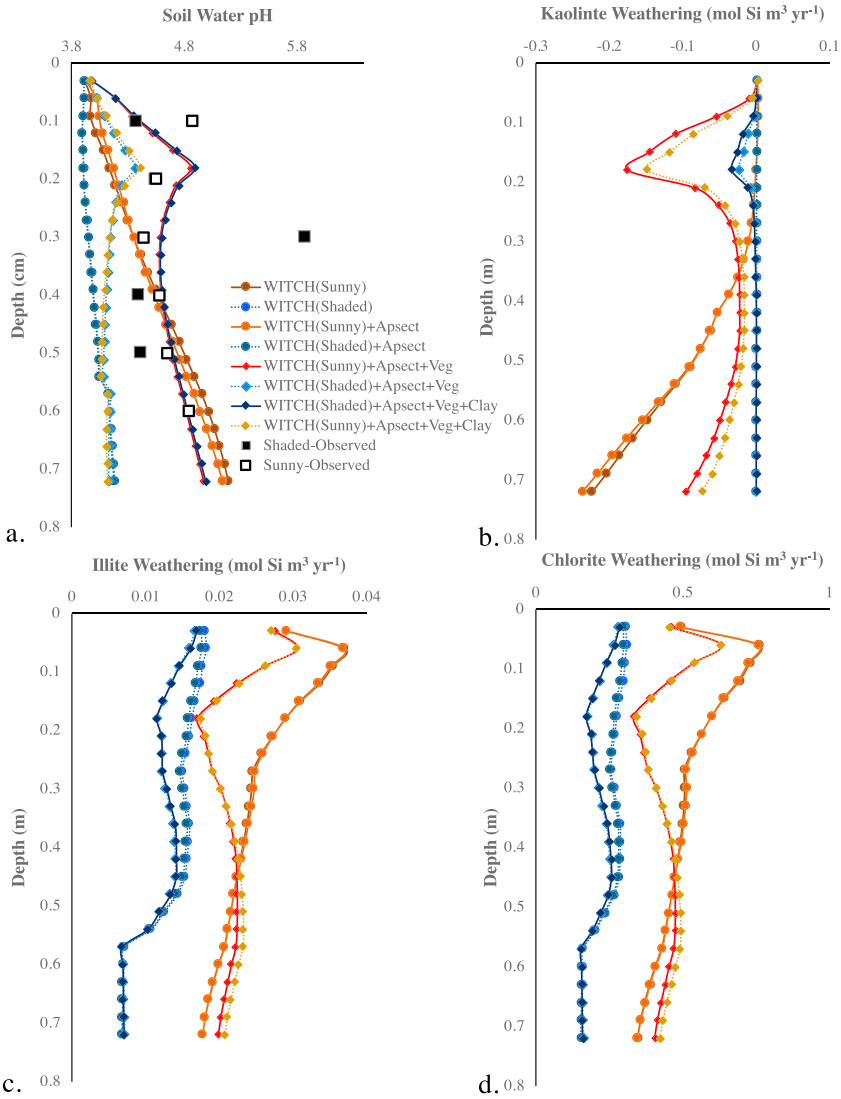

Figure 5. Average depth profiles of the observed (average measured soil water pH; sunny side, solid black squares; shaded side, open squares) and simulated soil water (a). pH and silica dissolved or precipitated from (b) kaolinite, (c) illite, and (d) chlorite weathering.

4.2. WITCH + Aspect Model

In contrast to the Baseline simulation where climate differs only minimally on the two sides of the catchment, in this section we assess weathering fluxes and mineral concentrations when differences in incoming solar radiation driven by topography are included. Specifically, the model was used to limit direct and diffuse solar radiation on the shaded hillslope by incorporating a topographic solar radiation module (see supporting information section 2) into the land surface hydrologic model (Flux-PIHM).

4.2.1. Hydrology in WITCH + Aspect

Overall, the inclusion of aspect resulted in cooler, wetter conditions on the shaded hillslope versus warmer, drier conditions on the sunny one. Specifically, the inclusion of aspect into Flux-PIHM led to a 0.8 °C difference in soil temperature: sunny side = 10.8 °C, shaded side = 10.0 °C (Figure 4b). In addition, the inclusion of aspect created wetter conditions (Figure 4c, average soil moisture was 0.154 cm^3/cm^3 with aspect, 1.5% greater than without aspect) on the shaded hillslope because of the lower latent heat flux (i.e., rate of evapotranspiration) and lower solar radiation. The inclusion of aspect also resulted in 100 mm/year more recharge to groundwater on the shaded versus the sunny side for equivalent drainage areas (Figure 4d and Table 2). During winter, differences in temperature can also result in modeled differences in freeze/thaw dynamics as

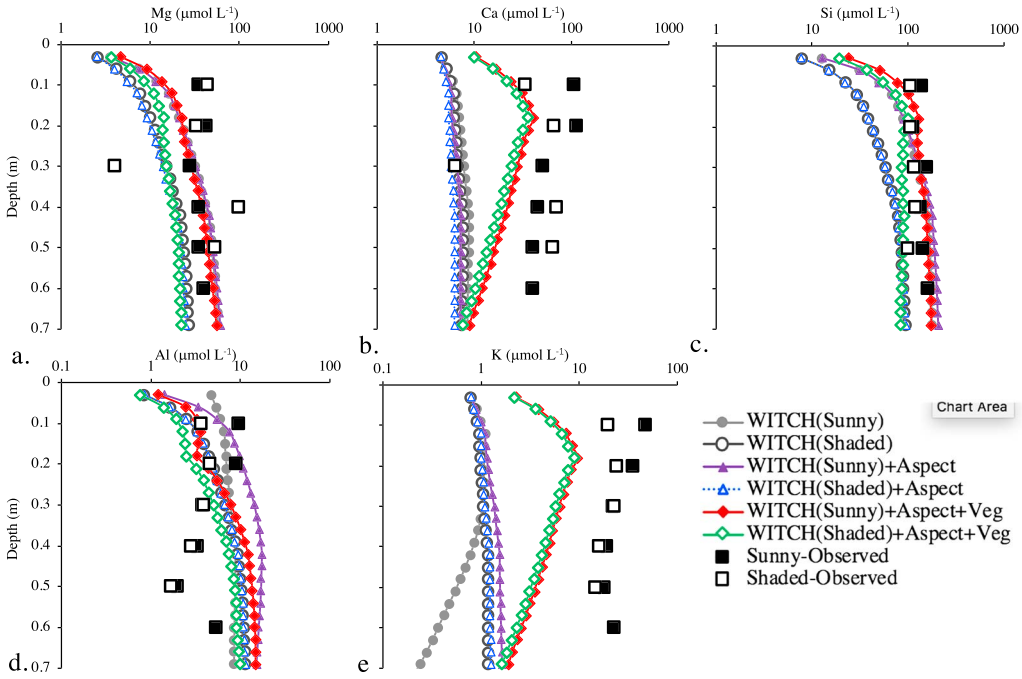

Figure 6. Observed (sunny side, solid black squares; shaded side, open squares) and modeled (colored) average soil water concentrations for (a) Mg, (b) Ca, (c) Si, (d) Al, and (e) K with depth averaged over the 6 years of the simulation (2006–2012). Simulations include the Baseline (sunny-gray, closed; shaded-gray, open), WITCH + Aspect (sunny-purple, closed; shaded-blue, open), and WITCH + Aspect + Vegetation (sunny-red, closed; shaded-green, open).

snow melt dynamics are governed by a simple temperature index, yet the warmer sunny hillslope still maintains a lower overall water flux compared to the shaded slope.

4.2.2. Weathering Fluxes

The soil solute concentrations on the shaded hillslope showed the same general seasonal and depth patterns as the WITCH-Baseline model (Figures 6a and 6c). However, with aspect included, less water now passed through the soil on the sunny hillslope. In this case with aspect, the solute weathering fluxes were nonetheless 110% greater on the sunny hillslope compared to the shaded one (Table 2). This greater weathering flux on the sunny hillslope—which more closely matched observations—resulted largely from the change in soil temperature between hillslope aspect (see black symbols in Figure 8b).

However, the inclusion of aspect also diluted the solute concentrations on both hillsides and shifted them away from observed values (see Figures 6 and 7). Thus, inclusion of aspect moved the estimated concentrations of Ca, K, and Si (Figures 6 and 7) further from the observations. NNSE values for all solutes remained fairly similar or slightly declined for all solutes except Al (which slightly increased, Table 3).

4.2.3. Mineral Weathering

Patterns in soil water saturation indices were similar between the WITCH-Baseline and WITCH + Aspect models, with soil water undersaturated with respect to illite, chlorite, albite, and K-feldspar but near equilibrium or supersaturated with respect to kaolinite (see, for example, Figures 5b–5d).

4.3. WITCH + Aspect + Vegetation Model

The simulated concentrations in soil solutions in all simulations presented so far for Ca, K, and Si were generally lower than observed (e.g., see Ca in Figure 6). Only Al was simulated to be generally higher than observed. On the other hand, Ca, K, and Si were also observed to be more concentrated in soil waters near the land surface than predicted by the model.

These observations led us to test if the addition of a module that described nutrient re-release at the land surface because of litter decomposition following elemental root uptake from the soil—biolifting by vegetation cycling of nutrients—could improve simulations of soil water concentrations and clay (illite, chlorite, and kaolinite) weathering. The basic idea of the cycling module, described more fully in section 3, was to

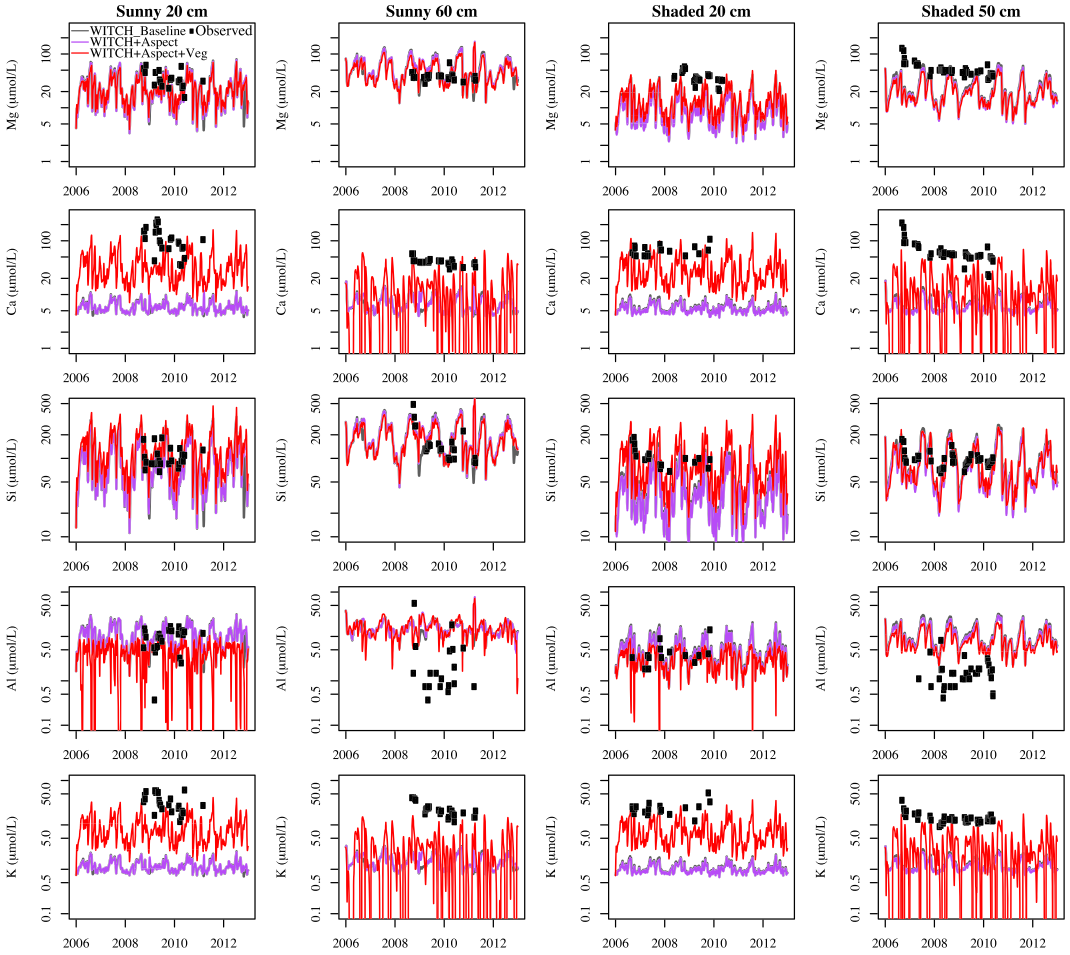

Figure 7. Comparison of observed (closed squares) and modeled (lines) soil solute water concentrations for (top to bottom) Mg, Ca, Si, Al, and K. Output from three simulations is compared for the sunny (left two columns) and shaded (right two columns) hillsides for shallow (20 cm) and deep (60 and 50 cm, respectively) soils: WITCH_ Baseline (gray), WITCH + Aspect (purple), and WITCH + Aspect + Veg (red). Given little discrepancy between WITCH_ Baseline and WITCH + Aspect, the simulations with Aspect often overlie the Baseline simulations.

account for the well-known phenomenon of biolifting and nutrient cycling of base cations and Si through vegetation. Specifically, Ca, K, Mg, and Si cycle through vegetation approximately 10–40 times before exiting soils and entering rivers (Uhlig et al., 2017). The cycling of soluble nutrient cations is expected to increase concentrations in the upper soil layers to a much greater extent than could be achieved through the chemical weathering of clay minerals alone in those upper layers. Of course, other potential processes not included in the model may also be happening as described in section 3.5.

4.3.1. Weathering Fluxes

The inclusion of the vegetation cycling module (WITCH + Aspect + Vegetation) impacts the soil water pH on the shaded and sunny slopes especially in the upper layers (e.g., Figures 9a and 9b). Specifically, from the

Table 3
Normalized Nash-Sutcliffe Efficiency (NNSE) Index for Model Soil Water Solute Concentrations Across the Entire Depth Profile

	Sunny (NPMS)					Shaded (SPMS)				
Models	Ca	Mg	K	Si	Al	Ca	Mg	K	Si	Al
WITCH_Baseline	0.152	0.266	0.085	0.373	0.116	0.156	0.201	0.122	0.171	0.091
WITCH + Aspect	0.153	0.262	0.085	0.366	0.104	0.155	0.198	0.121	0.165	0.109
WITCH + Aspec + Veg	0.208	0.295	0.106	0.421	0.136	0.194	0.201	0.162	0.229	0.156

Note. Values of 1 indicate a perfect model fit.

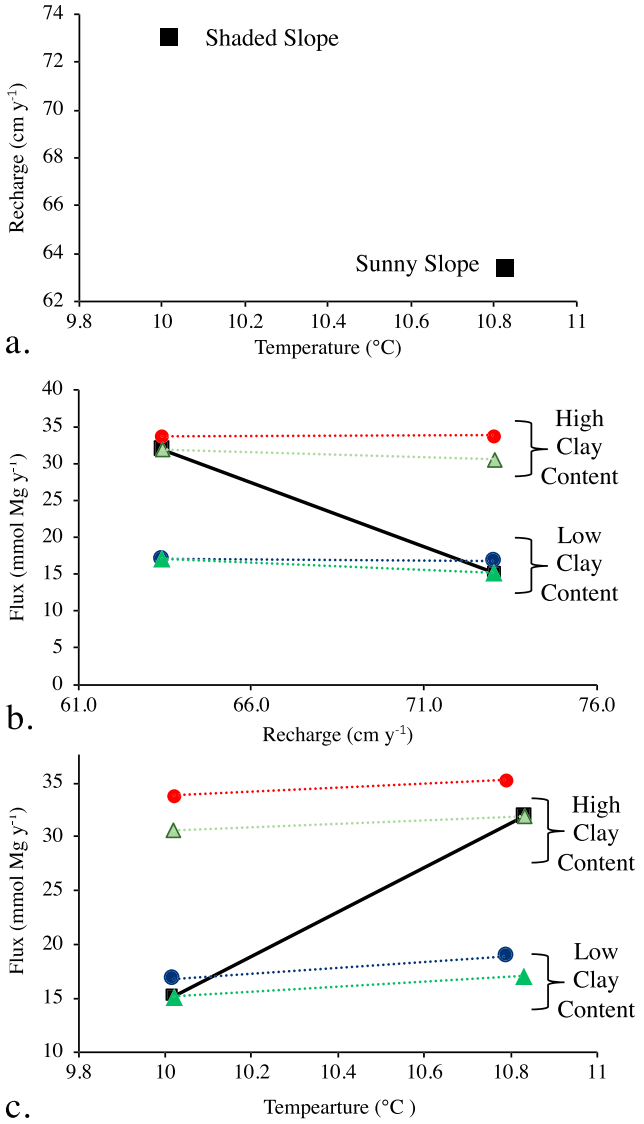

Figure 8. (a) Comparison between predicted values of recharge (water vertically infiltrating to a depth > 70 cm; m/year) and temperature (°C) on the sunny and shaded hillslopes for the WITCH + Aspect simulation. Relationship between simulated weathering fluxes (mmol Mg/year) compared to (b) recharge and (c) temperature for the WITCH + Aspect (black), WITCH + Aspect + High Clay (Red), WITCH + Aspect + High Clay + Vegetation Cycling (Dark Green), WITCH + Aspect + Low Clay (dark blue), and WITCH + Aspect + Low Clay + Vegetation cycling (light green). Standard deviation for fluxes is masked by point size (see Table 2).

surface down to about 20-cm depth, the pH rises rapidly, in agreement with the observed profiles. This part of the pH profile was not successfully mimicked in any of the previous simulations (Figure 5a). At depths greater than 40 cm, the pH profile for the sunny side remains in agreement with the observed values as noted for the WITCH + Aspect model described in the last section. In comparison, the shape of the simulated pH profile on the shaded slope more closely mirrors the observed trends with depth, albeit shifted slightly more acidic (Figure 5a). This increase in soil water pH in the model results from the increased production of alkalinity as more cations are released to solution during mineral dissolution.

The increase in NNSE values for all solutes with the inclusion of vegetation cycling (Table 3) indicates that the soil water solutes were better predicted when biolifting was included. The NNSE values for both the sunny and shaded hillslope slightly improved for soil water concentrations of Ca, Si, and Al, and the best match to observed values was produced in the near surface (< 40 cm) for both hillsides (Figure 7). The predictions of Mg were also slightly improved on the sunny hillslope with the addition of vegetation cycling because it produced a slight increase in concentration in the near surface soils (Figure 7). Incorporation of nutrient cycling also changed the saturation state of soil water with respect to minerals, which ultimately reduced the soil water solute Al concentrations (described below).

The output of the WITCH + Aspect + Vegetation model (Table 2 and Figures 6a–6c, 9b and 9c, and 9e and 9f) reveals weathering fluxes that are still 110% greater on the sunny side of the catchment, similar to the observations. Thus, both WITCH + Aspect and WITCH + Aspect + Vegetation are equivalently able to predict the higher aqueous weathering fluxes on the sunny side. However, with biolifting included, the Mg fluxes are about 10% less for both the sunny and shaded sides.

4.3.2. Mineral Weathering

Dissolution rates for chlorite and illite (mol Si·m^{-2} soil·year^{-1}) were diminished by 30–50% (Figures 4g and 4f) at depths shallower than 40 cm with the addition of vegetation cycling. This reduction in dissolution rate for Mg-rich minerals explains the slightly lower Mg concentrations simulated with the inclusion of vegetation cycling. At the same time, soil solutions that were near equilibrium with respect to kaolinite in the previous simulations were pushed to supersaturated conditions (Figure 4b). This increased the rate of precipitation of kaolinite by an order of magnitude, a phenomenon similar to observations previously made by Lucas (2001) for a different location.

The largest impact on weathering rates occurred during the warm growing season when litter decay rates are higher because of higher soil temperatures. During those periods, litter thus releases more cations to the soil. The main effect of vegetation cycling in the model is to increase soil water concentrations of nutrient elements and pH in the upper 20 cm of soil, in effect lowering the driving force for dissolution by moving topsoil water closer to equilibrium and increasing the production of kaolinite (Figure 5).

5. Discussion

5.1. Performance of Flux-PIHM-WITCH for Modeling Weathering Fluxes

By linking climatic forcing data (NLDAS-2), the land surface hydrologic model, Flux-PIHM, and the geochemical model WITCH, we built a baseline shale-weathering model (WITCH-Baseline) and compared soil water solute concentrations from model output to observations. In general, the models were able to

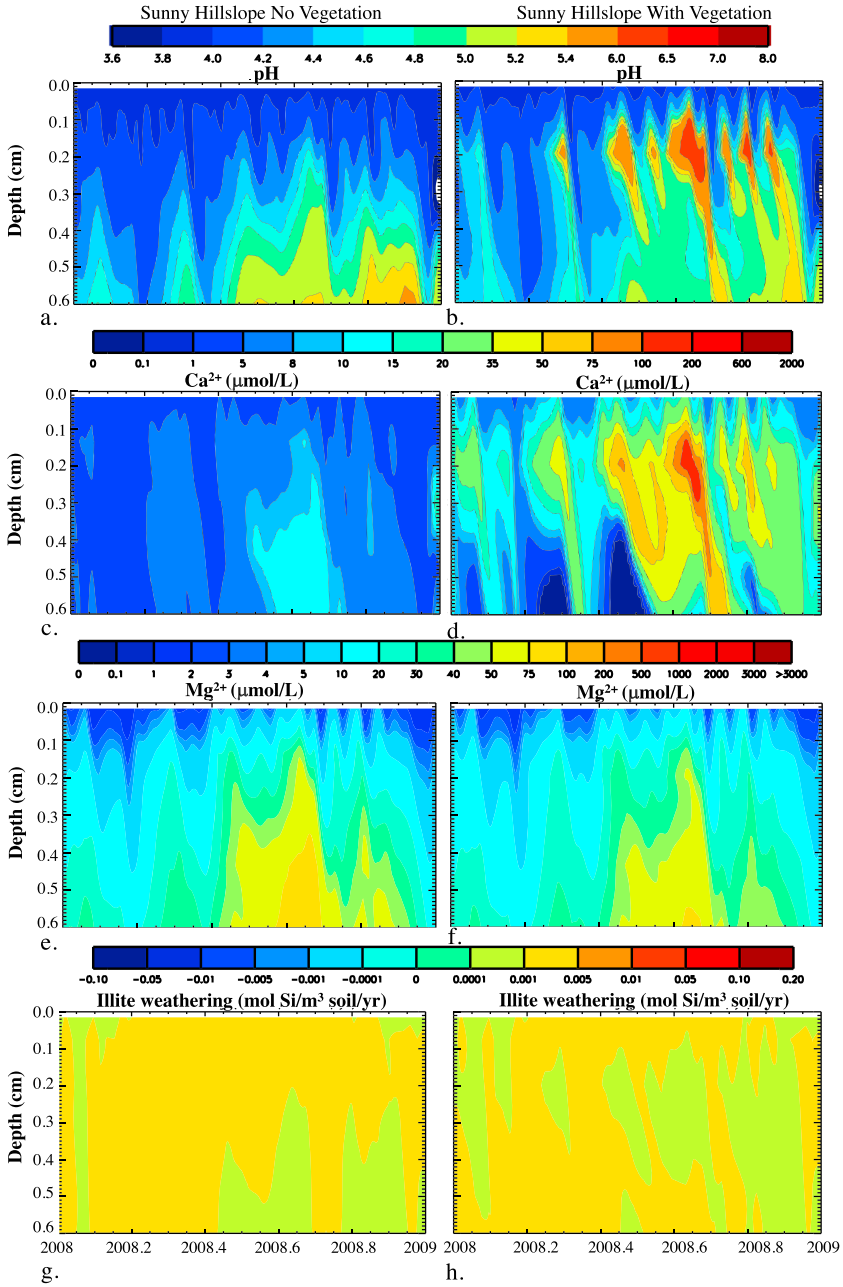

Figure 9. Simulated water soil profiles (0- to 60-cm deep) over 1 year (2008–2009). Each panel shows the plotted variable contoured (see legends) as a function of depth and time: (a and b) pH, (c and d) Ca concentrations, (e and f) Mg, and (g and h) illite saturation state. Results are from the WITCH + Aspect model (left column) and the WITCH + Aspect + Vegetation model (right column) on the sunny side of the catchment (clay content of soil = 10%). Warmer colors indicate higher pH, elevated Ca concentrations, elevated Mg concentrations, and greater potential for mineral dissolution (*x* axis is in decimal year, 0.2 represents 2.4 months).

simulate soil water solute concentrations within 30% for Mg and Si and within an order of magnitude for Ca, K, and Al (Figures 6 and 7). The model was best able to reproduce the observed Mg and Si soil water concentrations (Table 3). The pore water concentrations in the pedons on the two hillsides were more sensitive to the difference in clay contents and vegetation cycling than to differences in temperature (see Figure 10a and the discussion in section 5.2). The model predicted three observations: (i) the greater degree of variability in soil water solute concentrations on the shaded slope as compared to the sunny one; (ii) the higher weathering flux of the sunny side; and (iii) the depth variations in solutes in each pedon.

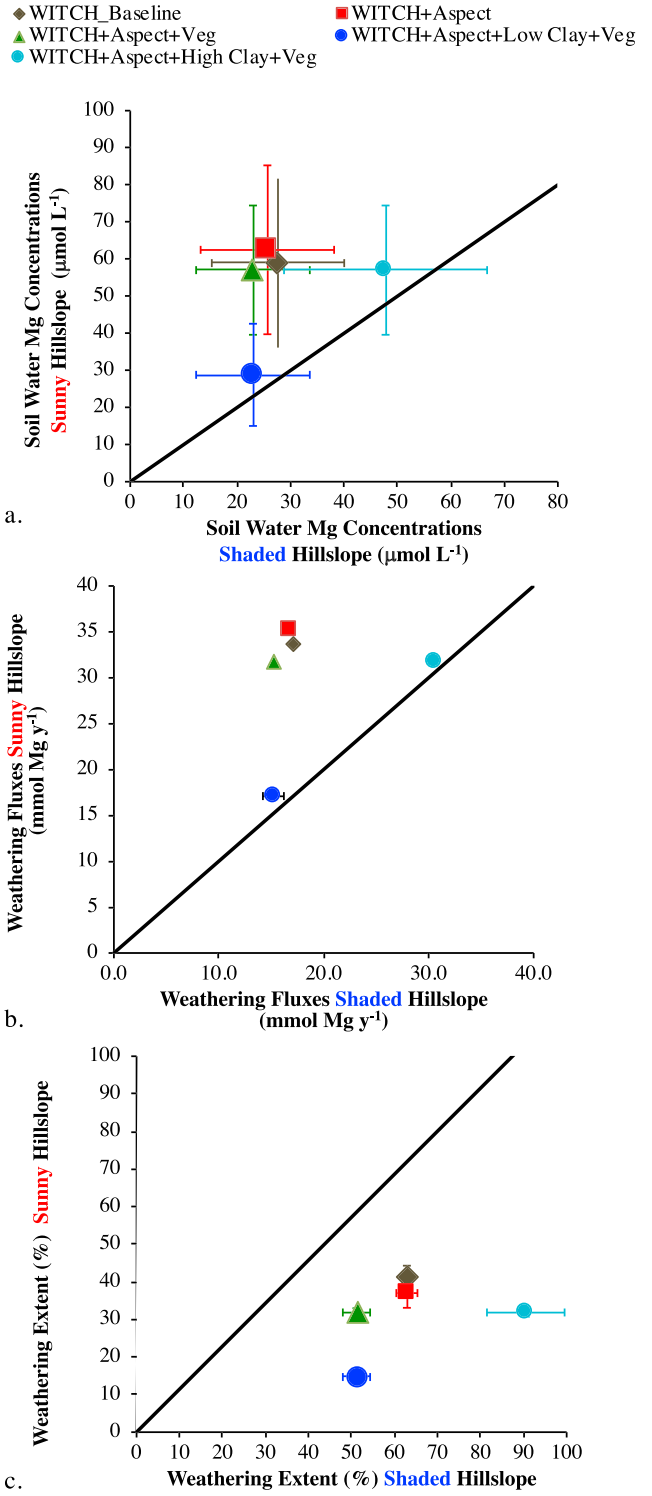

Figure 10. Comparison of (a) soil water Mg concentrations (μmol/L), (b) weathering fluxes (mmol Mg/year), and (c) weathering extent (%) for the sunny and shaded hillslopes. Error bars on the weathering fluxes (Figure 10b) are hidden by symbol. The black line represents a 1 to 1 line.

The model also simulated faster aqueous elemental release rates from dissolving minerals on the sunny hillside compared to the shaded one (Figure 10b). Modeled weathering fluxes are higher on the sunny hillside because that side has a higher temperature from increased solar radiation. They are also higher because the sunny side has inherited a higher clay content, but weathering fluxes were greatest on the sunny side even when clay content was held the same on both hillsides (Figure 10b). As argued explicitly below, it is possible that the difference in solar radiation is the ultimate cause of both higher weathering fluxes and higher clay content on the sunny side of the catchment.

Although WITCH + Aspect simulations were successful in showing a higher weathering flux on the sunny side, we needed to add nutrient cycling to reproduce the depth profiles of observed soil water solute concentrations of Ca and Al within an order of magnitude. Model output from WITCH + Aspect + Vegetation also improved the simulation of profiles of K, Mg, and Si (Table 3). Specifically, the inclusion of the vegetation cycling module raised soil water concentrations of base cations to as deep as 50 cm. This resulted in a small decline in primary mineral dissolution because of higher soil water concentrations and pH for cations, and this also resulted in a substantial increase in secondary mineral precipitation in the soils on both sides of the catchment. Thus, the addition of cation biolifting in the +Vegetation model through vegetation cycling slowed the rate of mass loss from the soil profile that would be produced if the only effects of vegetation included the effect of soil respiration and organic acid production. We emphasize that other effects of biota and organic matter are already simulated in WITCH even before the addition of the vegetation module. For example, clays and humic substances are modeled to retain cations in the upper soil horizons through sorption reactions that also affect pH, vegetation impacts the soil moisture, and both production of CO_2 through soil respiration and organic acids are modeled in the WITCH-Baseline and WITCH + Aspect models (Goddéris et al., 2006). Inclusion of the vegetation module simulates the additional process of biolifting by allowing uptake of base cations by roots and release back to the soil surface through decay of leaf material.

5.2. Implications

5.3. Dissolution Fluxes Decrease and Clay Precipitation Increases When Base Cations Are Uplifted by Vegetation

The role of vegetation in enhancing weathering through acid generation —both carbonic and organic—is a much better studied phenomenon than the effect on weathering of nutrient biolifting from depth toward the surface (e.g., Brantley & Olsen, 2014; Jobbágy & Jackson, 2001). In fact, the variation in these processes during ecosystem development can affect mineral weathering rates in shallow soils (e.g., Lawrence, Harden, & Maher, 2014,Lawrence, Steefel, & Maher, 2014). Recent work by Austin et al. (2018) shows that the translocation of K at depth to the surface by vegetation in a highly weathered, temperate forested ecosystem leads to the formation of 2:1 clays such as illite preferentially over 1:1 clays such as kaolinite, while work in rain forests have shown that cycling of Si by vegetation helps maintain kaolinite in the topsoil (Lucas, 2001; Lucas et al., 1993). Another phenomenon that is not included in our modeling is the effect of light molecular weight organic acids in promoting chemical weathering at shallow depths while inhibiting primary mineral weathering and increasing secondary mineral precipitation at greater

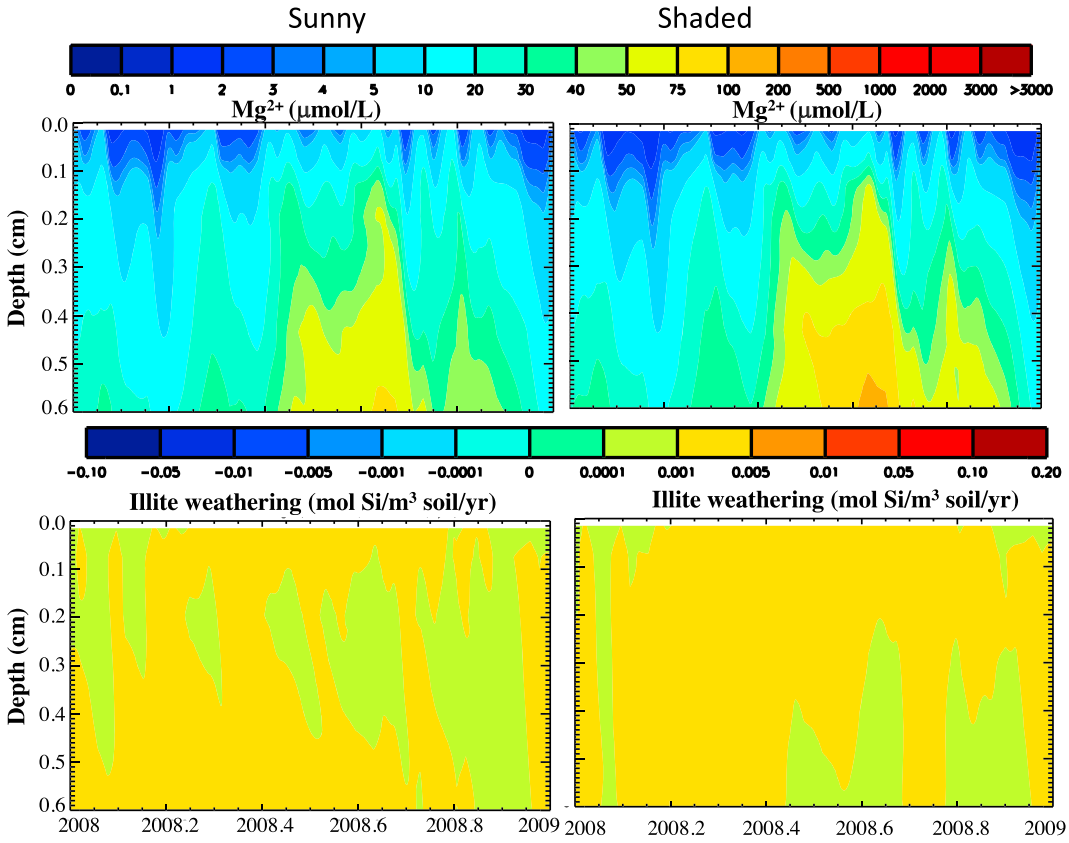

Figure 11. Simulated soil profiles (0- to 60-cm deep) over 1 year (2008–2009; *x* axis is in decimal year, 0.2 represents 2.4 months) for soil water Mg concentrations (top) and illite saturation state (bottom) for the sunny (left column) and shaded (right column) hillslopes under the WITCH + Aspect + High Clay + Vegetation model (for low clay content profiles see Figure SM4).

depths (Lawrence, Harden, & Maher, 2014; Lawrence et al., 2014). In addition, such effects of vegetation may not only alter the distribution of mineral abundances but may also change the hydraulic properties of the soil and thus the hydrology.

5.3.1. Weathering Flux Are More Sensitive to Differences in Aspect-Related Clay Content Than Microclimate

All of the calculated weathering fluxes were completed using present-day soil composition for the two sides of the catchment: sunny hillside = 10 wt % clay, shaded hillside = 3 wt % clay. Here we explore how such different clay contents can impact weathering fluxes. Specifically, we ran WITCH + Aspect + Vegetation after setting the grain size on both hillslopes to the same clay content—either high (10%) or low (3%).

The inclusion of high (10 wt %) versus low (3 wt %) clay content altered the concentrations of the solutes (e.g., Mg; Table 2 and Figures 11a and 11b, and SM4a and SM4b). Simulations indicated that chlorite weathering rates were nearly double under conditions of high versus low clay content (averaging 0.44 and 0.21 mol Si·m^3·year^{-1}, respectively).

When the clay content was increased, the solute concentrations were higher. This is expected because weathering rates increase with an increase in mineral surface area (see equation (1)). However, regardless of whether the clay content equaled 3 or 10 wt % the weathering fluxes were elevated on the sunny hillslope compared to the shaded one (weathering fluxes were 13% and 4% greater on the sunny hillslope for low and high clay content, respectively (Table 2 and Figure 8), with the former value being statistically significant in terms of exceeding two standard deviations from the mean). These simulations are consistent with a simulation previously made using the WITCH model for the loess profiles in the Mississippi River Valley (Goddéris et al., 2013). Specifically, Goddéris et al. (2013) projected an increase in silicate

weathering with an increase in temperature, which is to be expected based on the temperature dependence of silicate mineral dissolution kinetics as well as the temperature dependence of solubility. Thus, weathering fluxes are higher on the sunny side of the catchment both because of the higher temperature and the higher clay content.

5.4. Projecting Today's Mineral Weathering Rates to Illuminate How Past Processes Have Controlled Weathering Extent

An earthcast could be run over the full residence time of weathering for the soils to simulate the long-term weathering extent (Goddéris et al., 2010). However, that was beyond the scope of this work. Such a simulation, based on the current time step and processes represented in the model, would be computationally time intensive because the residence times of the midslope soils have been estimated from U isotopes to be 12 ± 3 ka for the sunny and 33 ± 24 ka for the shaded sides of Shale Hills (Ma et al., 2010). In comparison, we ran our earthcasting models for at most 6 years.

We nonetheless explore whether our modeling approach yields insights into the puzzle posed by Ma et al. (2013) about the long-term cation depletion in the soils from weathering. They observed that although the ongoing weathering fluxes appeared higher for the sunny side versus the shaded side, the fractional extent of depletion of the soil was higher on the shady side. We define the silicate weathering extent, W (unitless), as the fractional loss of material to weathering across all depths caused by reactions of chlorite, illite, albite, kaolinite, and K-feldspar. The value was calculated here from the model-derived dissolution rates integrated over the soil residence time divided by the original Si content in the comparable volume of parent material (Si_{pm}; mol Si/m^3). To calculate W from solid profiles, we first determined the average annual net loss rate of Si from each mineral ($R_{Si,m}$; mol Si·m^{-3}·year^{-1}) based on the solid phase simulations. We then summed these values over the five minerals (m), multiplied the sum by the residence time for the soil (t; ka), and then divided that value by the silica content in the same volume of parent material (18,031 mol Si/m^3):

$$W = \frac{t \times \sum_{m=0}^{5} R_{Si,m}}{Si_{pm}} \tag{4}$$

This approach uses the net Si weathering flux calculated for today's conditions using WITCH and then integrates it over the soil residence time as if the flux stayed constant.

Even though the aqueous weathering fluxes were predicted to be faster on the sunny side of the catchment compared to the shaded one (Table 2), values of W were greater on the shaded than the sunny hillside when the residence times from Ma et al. (2013) were used (Figure 10c and Table 2): the value of W calculated for the sunny side was 0.32 while for the shaded side it was 0.51. Furthermore, these calculations show a greater weathering extent on the shaded slope compared to the sunny one regardless of clay content (Figures 9c, 10c, and 10d). This difference was simply because of the longer residence time of soils on the shaded side. In fact, if we use equation (4) and assume the residence time for the sunny-side soil is 12 ka but the residence time of the shady-side soil equals any value higher than 22 ka, then W is always higher for the shaded side soil.

At face value, then, this calculation and our modeling approach suggest that faster weathering fluxes that are observed on the sunny side of the catchment are best attributed to the higher solar radiation (temperature effect on dissolution) and the higher clay content. In contrast, the greater extent of weathering on the shaded side is because of the longer residence time of soils on the shaded side (Figure 10c).

This discussion has some intriguing implications. Apparently, the lower clay content on the shady side is not a result of faster weathering on that side. It is only the result of the slower physical removal of regolith on that side of the catchment and the longer residence times (see West et al., 2013). However, assuming a constant model-calculated weathering rate for the 10% clay scenario over a time period of somewhere between 4 and 8 ka, the clay content would be reduced to 3% on the sunny side (that is an overestimate because the calculation should include constant updating of dissolution rate as a function of mineral surface area). In other words, the differences in residence times for the soils on either side of the catchment are likely able to explain not only the differences in weathering extent but also the differences in clay content. To accurately determine mineral dissolution over millennial projections, we therefore must be able to account for the change in dissolution rates as clay content evolves.

6. Conclusions

The WITCH + Aspect + Vegetation cycling simulations demonstrated that chemical weathering fluxes in a shale catchment are more sensitive to clay size distribution and biolifting of base cations than microclimate difference alone. Furthermore, these differences in clay content were also likely to have emerged over thousands of years as a result of aspect. Together, these simulations help to potentially explain the greater extent of weathering observed on the shaded side of the basin, while also elucidating why we observe faster elemental release rates on the sunny slopes at Shale Hills. Our work suggests that the faster elemental release rates can result from aspect-driven differences in clay content and elevated temperatures on the sunny side.

Matching of observed and predicted soil water solute concentrations required the inclusion of a vegetation cycling module (specifically the inclusion of biolifting) in WITCH. Surprisingly, biolifting reduced shale weathering by 10%. These observations have implications for earthcasting the future effect of climate on weathering. For example, accounting for the impact of vegetation-driven nutrient uplift on mass loss may have a significant impact on earthcasts of weathering fluxes especially where land cover and land use may be changing. In addition, the translocation of nutrients from depth to the surface is likely to be a common occurrence in many ecosystems, but the effect of this translocation of nutrients could depend on the degree to which a system is weathered, the nature of the ecosystem (aggrading, degrading, and steady state), the climatic conditions, or human activities. Several researchers have argued, for example, that net primary production of forests may increase in the coming decades because of increased CO_2 fertilization (Norby et al., 2005), but how this will affect mineral abundances and weathering rates in surface soils will be a complicated interplay of many factors. Here we present one approach toward earthcasting, bringing together short- and long-time scale data from the same location to help constrain the trajectory of earth system processes as we face the changing dynamics of the water and carbon cycle during the Anthropocene.

Acknowledgments
This work was facilitated by NSF Critical Zone Observatory program grants to C. J. D. (EAR 07-25019) and S. L. B. (EAR 12-39285 and EAR 13-31726). The research was conducted in Penn State's Stone Valley Forest, which is supported and managed by Penn State's Forestland Management Office in the College of Agricultural Sciences. X. Gu was supported by DOE grant DE-FG02-05ER15675. Data and PIHM model output used to parameterize, calibrate, and validate the model can be found through the Critical Zone Observatory websites criticalzone.org and http://www.czo.psu.edu/data_geochemical_geophysical.html. We acknowledge conversations with N. West and would like to thank the reviewers, including C. Harman, for their thoughtful and insightful comments.

References

Andrews, D. M., Lin, H., Zhu, Q., Jin, L., & Brantley, S. L. (2011). Hot spots and hot moments of dissolved organic carbon export and soil organic carbon storage in the Shale Hills catchment. *Vadose Zone Journal*, *10*(3), 943–954. https://doi.org/10.2136/vzj2010.0149

Austin, J. C., Perry, A., Richter, D. D., & Schroeder, P. A. (2018). Modifications of 2:1 clay minerals in kaolinite-dominated Ultisos under changing land-use regimes. *Clays and Clay Minerals*, *66*(1), 61–73.

Brantley, S. L., Holleran, M. E., Jin, L., & Bazilevskaya, E. (2013). Probing deep weathering in the Shale Hills Critical Zone Observatory, Pennsylvania (USA): The hypothesis of nested chemical reaction fronts in the subsurface. *Earth Surface Processes and Landforms*, *38*(11), 1280–1298. https://doi.org/10.1002/esp.3415

Brantley, S. L., & Olsen, A. A. (2014). Reaction kinetics of primary rock-forming minerals under ambient conditions. In H. D. Holland, & K. Turekian (Eds.), *Treatise on geochemistry*, (pp. 69–113). Oxford: Elsevier. https://doi.org/10.1016/B978-0-08-095975-7.00503-9

Casanova, M., Messing, I., & Joel, A. (2000). Influence of aspect and slope gradient on hydraulic conductivity measured by tension infiltrometer. *Hydrological Processes*, *14*(1), 155–164. https://doi.org/10.1002/(SICI)1099-1085(200001)14:1<155::AID-HYP917>3.0.CO;2-J

Chen, H., & Tain, H. Q. (2005). Does a general temperature-dependent Q10 model of soil respiration exist at biome and global scale? *Journal of Integrative Plant Biology*, *47*(11), 1288–1302. https://doi.org/10.1111/j.1744-7909.2005.00211.x

Chorover, J., Troch, P. A., Rasmussen, C., Brooks, P. D., Pelletier, J. D., Breshears, D. D., et al. (2011). How water, carbon, and energy drive critical zone evolution: The Jemez–Santa Catalina Critical Zone Observatory. *Vadose Zone Journal*, *10*(3), 884–899. https://doi.org/10.2136/vzj2010.0132

Drever, J. I. (1988). *The geochemistry of natural waters*, (Vol. 437). Englewood Cliffs: Prentice Hall.

Duffy, C., Shi, Y., Davis, K., Slingerland, R., Li, L., Sullivan, P. L., et al. (2014). Designing a suite of models to explore critical zone function. *Procedia Earth and Planetary Science*, *10*, 7–15. https://doi.org/10.1016/j.proeps.2014.08.003

Fan, Y., Clark, M., Lawrence, D., Swenson, S., Band, L., Brantley, S. L., et al. (2018). Structures and functions of hillslope hydrology with relevance to Earth system modeling: Syntheses and testable hypotheses. *Water Resources Research*, *55*, 1737–1772. https://doi.org/10.1029/2018WR023903

Gaines, K. P., Stanley, J. W., Meinzer, F. C., McCulloh, K. A., Woodruff, D. R., Chen, W., et al. (2015). Reliance on shallow soil water in a mixed-hardwood forest in central Pennsylvania. *Tree Physiology*, *36*(4), 444–458. https://doi.org/10.1093/treephys/tpv113

Geroy, I. J., Gribb, M. M., Marshall, H. P., Chandler, D. G., Benner, S. G., & McNamara, J. P. (2011). Aspect influences on soil water retention and storage. *Hydrological Processes*, *25*(25), 3836–3842. https://doi.org/10.1002/hyp.8281

Goddéris, Y., & Brantley, S. L. (2013). Earthcasting the future critical zone. *Elem Sci Anth*, *1*. https://doi.org/10.12952/journal.elementa.000019

Goddéris, Y., Brantley, S. L., François, L. M., Schott, J., Pollard, D., Déqué, M., & Dury, M. (2013). Rates of consumption of atmospheric CO_2 through the weathering of loess during the next 100 yr of climate change. *Biogeosciences*, *10*(1), 135–148. https://doi.org/10.5194/bg-10-135-2013

Goddéris, Y., François, L. M., Probst, A., Schott, J., Moncoulon, D., Labat, D., & Viville, D. (2006). Modelling weathering processes at the catchment scale: The WITCH numerical model. *Geochimica et Cosmochimica Acta*, *70*(5), 1128–1147. https://doi.org/10.1016/j.gca.2005.11.018

Goddéris, Y., Williams, J. Z., Schott, J., Pollard, D., & Brantley, S. L. (2010). Time evolution of the mineralogical composition of Mississippi Valley loess over the last 10 kyr: Climate and geochemical modeling. *Geochimica et Cosmochimica Acta*, *74*(22), 6357–6374. https://doi.org/10.1016/j.gca.2010.08.023

Gupta, H. V., Kling, H., Yilmaz, K. K., & Martinez, G. F. (2009). Decomposition of the mean squared error and NSE performance criteria: Implications for improving hydrological modelling. *Journal of Hydrology*, *377*(1–2), 80–91. https://doi.org/10.1016/j.jhydrol.2009.08.003

Hasenmueller, E. A., Gu, X., Weitzman, J. N., Adams, T. S., Stinchcomb, G. E., Eissenstat, D. M., et al. (2017). Weathering of rock to regolith: The activity of deep roots in bedrock fractures. *Geoderma*, *300*, 11–31. https://doi.org/10.1016/j.geoderma.2017.03.020

Hasenmueller, E. A., Jin, L., Stinchcomb, G. E., Lin, H., Brantley, S. L., & Kaye, J. P. (2015). Topographic controls on the depth distribution of soil CO_2 in a small temperate watershed. *Applied Geochemistry*, *63*, 58–69. https://doi.org/10.1016/j.apgeochem.2015.07.005

Herndon, E. M. (2012). Biogeochemistry of manganese contamination in a temperate forested watershed.

Herndon, E. M., Dere, A. L., Sullivan, P. L., Norris, D., Reynolds, B., & Brantley, S. L. (2015). Landscape heterogeneity drive contrasting concentration-discharge relationships in shale headwater catchments. *Hydrology and Earth System Sciences*, *19*(8), 3333–3347. https://doi.org/10.5194/hess-19-3333-2015

Herndon, E. M., Jin, L., Andrews, D. M., Eissenstat, D. M., & Brantley, S. L. (2015). Importance of vegetation for manganese cycling in temperate forested watersheds. *Global Biogeochemical Cycles*, *29*, 160–174. https://doi.org/10.1002/2014GB004858

Hinckley, E. L. S., Barnes, R. T., Anderson, S. P., Williams, M. W., & Bernasconi, S. M. (2014). Nitrogen retention and transport differ by hillslope aspect at the rain-snow transition of the Colorado Front Range. *Journal of Geophysical Research: Biogeosciences*, *119*, 1281–1296. https://doi.org/10.1002/2013JG002588

Hinckley, E. L. S., Ebel, B. A., Barnes, R. T., Anderson, R. S., Williams, M. W., & Anderson, S. P. (2014). Aspect control of water movement on hillslopes near the rain–snow transition of the Colorado Front Range. *Hydrological Processes*, *28*(1), 74–85. https://doi.org/10.1002/hyp.9549

Jin, L., Andrews, D. M., Holmes, G. H., Lin, H., & Brantley, S. L. (2011). Opening the "black box": Water chemistry reveals hydrological controls on weathering in the Susquehanna Shale Hills Critical Zone Observatory. *Vadose Zone Journal*, *10*(3), 928–942. https://doi.org/10.2136/vzj2010.0133

Jin, L., Ravella, R., Ketchum, B., Bierman, P. R., Heaney, P., White, T., & Brantley, S. L. (2010). Mineral weathering and elemental transport during hillslope evolution at the Susquehanna/Shale Hills Critical Zone Observatory. *Geochimica et Cosmochimica Acta*, *74*(13), 3669–3691. https://doi.org/10.1016/j.gca.2010.03.036

Jobbágy, E. G., & Jackson, R. B. (2001). The distribution of soil nutrients with depth: Global patterns and the imprint of plants. *Biogeochemistry*, *53*(1), 51–77. https://doi.org/10.1023/A:1010760720215

Kumar, M. (2009). Toward a hydrologic modeling system. Ph.D. thesis, The Pennsylvania State University, 251 pp.

Kunkel, M. L., Flores, A. N., Smith, T. J., McNamara, J. P., & Benner, S. G. (2011). A simplified approach for estimating soil carbon and nitrogen stocks in semi-arid complex terrain. *Geoderma*, *165*(1), 1–11. https://doi.org/10.1016/j.geoderma.2011.06.011

Lawrence, C., Harden, J., & Maher, K. (2014). Modeling the influence of organic acids on soil weathering. *Geochimica et Cosmochimica Acta*, *139*, 487–507. https://doi.org/10.1016/j.gca.2014.05.003

Lawrence, C., Steefel, C., & Maher, K. (2014). Abiotic/biotic coupling in the rhizosphere: A reactive transport modeling analysis. *Procedia Earth and Planetary Science*, *10*, 104–108. https://doi.org/10.1016/j.proeps.2014.08.037

Li, L., Bao, C., Sullivan, P. L., Brantley, S., Shi, Y., & Duffy, C. (2017). Understanding watershed hydrogeochemistry: 2. Synchronized hydrological and geochemical processes drive stream chemostatic behavior. *Water Resources Research*, *53*, 2346–2367. https://doi.org/10.1002/2016WR018935

Lin, H. (2006). Temporal stability of soil moisture spatial pattern and subsurface preferential flow pathways in the Shale Hills Catchment. *Vadose Zone Journal*, *5*(1), 317–340. https://doi.org/10.2136/vzj2005.0058

Lin, H. S., Kogelmann, W., Walker, C., & Bruns, M. A. (2006). Soil moisture patterns in a forested catchment: A hydropedological perspective. *Geoderma*, *131*(3-4), 345–368. https://doi.org/10.1016/j.geoderma.2005.03.013

Lucas, Y. (2001). The role of plants in controlling rates and products of weathering: Importance of biological pumping. *Annual Review of Earth and Planetary Sciences*, *29*(1), 135–163. https://doi.org/10.1146/annurev.earth.29.1.135

Lucas, Y., Luizao, F. J., Chauvel, A., Rouiller, J., & Nahon, D. (1993). The relation between biological activity of the rain forest and mineral composition of soils. *Science*, *260*(5107), 521–523. https://doi.org/10.1126/science.260.5107.521

Ma, L., Chabaux, F., Pelt, E., Blaes, E., Jin, L., & Brantley, S. (2010). Regolith production rates calculated with uranium-series isotopes at Susquehanna/Shale Hills Critical Zone Observatory. *Earth and Planetary Science Letters*, *297*(1-2), 211–225. https://doi.org/10.1016/j.epsl.2010.06.022

Ma, L., Chabaux, F., West, N., Kirby, E., Jin, L., & Brantley, S. (2013). Regolith production and transport in the Susquehanna Shale Hills Critical Zone Observatory, Part 1: Insights from U-series isotopes. *Journal of Geophysical Research: Earth Surface*, *118*, 722–740. https://doi.org/10.1002/jgrf.20037

Meinzer, F. C., Woodruff, D. R., Eissenstat, D. M., Lin, H. S., Adams, T. S., & McCulloh, K. A. (2013). Above-and belowground controls on water use by trees of different wood types in an eastern US deciduous forest. *Tree Physiology*, *33*(4), 345–356. https://doi.org/10.1093/treephys/tpt012

Murray, A. B., Lazarus, E., Ashton, A., Baas, A., Coco, G., Coulthard, T., et al. (2009). Geomorphology, complexity, and the emerging science of the Earth's surface. *Geomorphology*, *103*(3), 496–505. https://doi.org/10.1016/j.geomorph.2008.08.013

Norby, R. J., DeLucia, E. H., Gielen, B., Calfapietra, C., Giardina, C. P., King, J. S., et al. (2005). Forest response to elevated CO_2 is conserved across a broad range of productivity. *Proceedings of the National Academy of Sciences*, *102*(50), 18,052–18,056. https://doi.org/10.1073/pnas.0509478102

Nossent, J., & Bauwens, W. (2012). Application of a normalized Nash-Sutcliffe efficiency to improve the accuracy of the Sobol' sensitivity analysis of a hydrological model. In EGU General Assembly Conference Abstracts (Vol. 14, p. 237).

Pelletier, J. D., Barron-Gafford, G. A., Breshears, D. D., Brooks, P. D., Chorover, J., Durcik, M., et al. (2013). Coevolution of nonlinear trends in vegetation, soils, and topography with elevation and slope aspect: A case study in the sky islands of southern Arizona. *Journal of Geophysical Research: Earth Surface*, *118*, 741–758. https://doi.org/10.1002/jgrf.20046

Pelletier, J. D., Barron-Gafford, G. A., Gutiérrez-Jurado, H., Hinckley, E. L. S., Istanbulluoglu, E., McGuire, L. A., et al. (2018). Which way do you lean? Using slope aspect variations to understand critical zone processes and feedbacks. *Earth Surface Processes and Landforms*, *43*(5), 1133–1154. https://doi.org/10.1002/esp.4306

Pelletier, J. D., Brad Murray, A., Pierce, J. L., Bierman, P. R., Breshears, D. D., Crosby, B. T., et al. (2015). Forecasting the response of Earth's surface to future climatic and land use changes: A review of methods and research needs. *Earth's Future*, *3*(7), 220–251. https://doi.org/10.1002/2014EF000290

Schott, J., Pokrovsky, O. S., & Oelkers, E. H. (2009). The link between mineral dissolution/precipitation kinetics and solution chemistry. *Reviews in Mineralogy and Geochemistry*, *70*(1), 207–258. https://doi.org/10.2138/rmg.2009.70.6

Shi, Y., Davis, K. J., Duffy, C. J., & Yu, X. (2013). Development of a coupled land surface hydrologic model and evaluation at a critical zone observatory. *Journal of Hydrometeorology*, *14*(5), 1401–1420. https://doi.org/10.1175/JHM-D-12-0145.1

Sullivan, P. L., Hynek, S. A., Gu, X., Singha, K., White, T., West, N., et al. (2016). Oxidative dissolution under the channel leads geomorphological evolution at the Shale Hills catchment. *American Journal of Science*, *316*(10), 981–1026. https://doi.org/10.2475/10.2016.02

Sullivan, P. L., Li, L., Goddéris, Y., Brantley, S. L. (2018). Poised to hindcast and arthcast the effect of climate on the critical zone: Shall Hills as a model. *In* Biogeochemical Cycles: Ecological Drivers and Environmental Impact.

Sullivan, P. L., Ma, L., West, N., Jin, L., Karwan, D. L., Noireaux, J., et al. (2016). CZ-tope at Susquehanna Shale Hills CZO: Synthesizing multiple isotope proxies to elucidate critical zone processes across timescales in a temperate forested landscape. *Chemical Geology*, *445*, 103–119. https://doi.org/10.1016/j.chemgeo.2016.05.012

Sverdrup, H. (1996). Geochemistry, the key to understanding environmental chemistry. *Science of the Total Environment*, *183*(1–2), 67–87. https://doi.org/10.1016/0048-9697(95)04978-9

Sverdrup, H., & Warfvinge, P. (1995). Estimating field weathering rates using laboratory kinetics. *Reviews in Mineralogy and Geochemistry*, *31*(1), 485–541.

Thomas, E. M., Lin, H., Duffy, C. J., Sullivan, P. L., Holmes, G. H., Brantley, S. L., & Jin, L. (2013). Spatiotemporal patterns of water stable isotope compositions at the Shale Hills Critical Zone Observatory: Linkages to subsurface hydrologic processes. *Vadose Zone Journal*, *12*(4). https://doi.org/10.2136/vzj2013.01.0029

Uhlig, D., Schuessler, J. A., Bouchez, J., Dixon, J. L., & von Blanckenburg, F. (2017). Quantifying nutrient uptake as driver of rock weathering in forest ecosystems by magnesium stable isotopes. *Biogeosciences*, *14*(12), 3111–3128. https://doi.org/10.5194/bg-14-3111-2017

West, N., Kirby, E., Bierman, P., Slingerland, R., Ma, L., Rood, D., & Brantley, S. (2013). Regolith production and transport at the Susquehanna Shale Hills Critical Zone Observatory, part 2: Insights from meteoric 10Be. *Journal of Geophysical Research: Earth Surface*, *118*, 1877–1896. https://doi.org/10.1002/jgrf.20121